Electronic Supplementary Information

Asymmetric Electrodes with Transition Metal Disulfides Heterostructure and Amorphous Bimetallic Hydroxide for Effective Alkaline Water Electrolysis

Xiao Hu Wang [a], Yu Ling [a], Bang Lin Li [a], Xiao Lin Li [a], Guo Chen [a], Bai Xiang Tao [a], Ling Jie Li [b], Nian Bing Li *[a], and Hong Qun Luo *[a]

[a] School of Chemistry and Chemical Engineering, Southwest University, Chongqing 400715, P.R. China.

[b] College of Chemistry and Chemical Engineering, Chongqing University, Chongqing 400044, P.R. China.

***Corresponding authors.** Tel./fax: +86 23 6825 3237

E-mail addresses: linb@swu.edu.cn; luohq@swu.edu.cn

Experimental

General

All reagents were purchased from chemical vendors and used without further purification. Carbon cloth (CC) was purchased from Taiwan CeTech Co., Ltd. Sodiummolybdate dihydrate $Na_2MoO_4{\cdot}2H_2O$, nickel(II) chloride hexahydrate ($NiCl_2{\cdot}6H_2O$), and ruthenium (IV) oxide (RuO_2) were purchased from Sigma-Aldrich, Co., LLC. Shanghai, China. Iron(III) chloride hexahydrate ($FeCl_3{\cdot}6H_2O$), ammonium sulfate ($(NH_4)_2SO_4$), sodium hypophosphite monohydrate ($NaPO_2H_2{\cdot}H_2O$), and sublimed sulfur (S) were purchased from Chengdu Kelong Chemical Factory (Chengdu, China). Potassium hydroxide (KOH), ethanol, acetone, edetate disodium (EDTA-Na_2), nitric acid (wt 68% (HNO_3)), sodium nitrate ($NaNO_3$), and sulfuric acid (wt 98% (H_2SO_4)) were purchased from Chongqing Chuandong Chemical (Group) Co., Ltd. (China). Thiourea was purchased from Aladdin Industrial Corporation. Ethylenediamine was purchased from Shanghai Macklin Biochemical Co., Ltd. Nafion (5 wt %) was purchased from Alfa Aesar (China) Chemical Co., Ltd. Pt/C (20 wt % Pt on Vulcan XC-72R) was purchased from Johnson Matthey (Shanghai) Chemical Co., Ltd. Ultrapure water (> 18.2 MΩ cm) was provided by an AquaPro AD2C-00-OR laboratory ultrapure water machine.

X-ray diffraction (XRD) was recorded on a Shimadzu XRD-7000S X-ray diffractometer (Shimadzu, Japan) using Cu Kα radiation (λ = 1.5418 Å). Raman spectrum (Renishaw, InVia, UK) was recorded over the frequency range of 100-1000 cm^{-1} using a 20 mW air-cooled argon ion laser (532.8 nm). Scanning electron microscopy (SEM) was performed on an SU 8010 FE-SEM (Hitachi, Japan). Transmission electron microscope (TEM) and high-angle annular dark-field scanning transmission electron microscopy (HAADF-STEM) images were performed on a Tecnai G2-F20 microscope equipped with a field emission gun operating at 200 kV (FEI Corporation, USA). X-ray photoelectron spectroscopy (XPS) study was performed on a Thermo Fisher Scientific ESCALAB 250Xi X-ray photoelectron spectrometer with a monochromatic X-ray source gun type (Al Kα hυ =1486.6 eV) (Thermo Fisher Scientific, USA).

All the electrochemical measurements were performed using a CHI660E electrochemical workstation at room temperature in a three-electrode electrochemical system (CH Instruments Inc, Shanghai, China). Platinum plate as the counter electrode, Ag/AgCl electrode in saturated KCl solution as the reference electrode, Ni_3S_2/MoS_2-CC and $NiFe(OH)_x@Ni_3S_2/MoS_2$-CC (size: 1 cm × 1

cm) as the working electrodes. Long-time durability test was performed using chronoamperometry at fixed potentials (graphite rod as the counter electrode). All HER/OER measurements are in progress 1.0 M KOH after purification by infusing saturated O_2. Linear sweep voltammetry (LSV) and cyclic voltammetry (CV) of Ni_3S_2/MoS_2-CC and $NiFe(OH)_x@Ni_3S_2/MoS_2$-CC for HER/OER were conducted with a scan rate of 5 mV s^{-1}. Data presented in polarization curves and corresponding Tafel plots were all iR-corrected and carried out at 5 mV s^{-1}. The electrochemical active surface area (ECSA) was determined from the CV data with an optimized potential window at different scan rates (20, 40, 60, 80, 100, and 120 mV s^{-1}). When plotting the Δj (= $j_{anode} - j_{cathode}$) vs. RHE against the scan rate, a linear slope that was twice of the double layer capacitance (C_{dl}) was used to calculate the ECSA. Electrochemical impedance spectroscopy (EIS) was performed in the frequency range of 100 kHz to 0.01 Hz with an amplitude of 5 mV. For water electrolysis, two-electrode electrolyzer was constructed using Ni_3S_2/MoS_2-CC and $NiFe(OH)_x@Ni_3S_2/MoS_2$-CC as the cathode and anode, respectively. The recorded potentials were adjusted by the equation: E(RHE) = E(Ag/AgCl) + (0.2012 + 0.059 pH) V. The turnover frequency (TOF) value is calculated from equation TOF (s^{-1}) = ($j \times A$)/($4 \times F \times n$) in which j (A cm^{-2}) represents the measured current density at overpotential of 340 mV, A (cm^2) represents the area of CC-based electrodes, F represents the Faraday constant (96485.3 C mol^{-1}), number 4 means that 4 electrons are required to generate one molecule of O_2, and n represents the moles of coated metal atom.

Synthesis of MoS_2-CC

Typically, CC (1 cm × 1.5 cm) was treated with HNO_3, ultrapure water, acetone, and ethanol for several times and dried at 60 °C for overnight before use. Then, 0.061 g of $Na_2MoO_4 \cdot 2H_2O$ and 0.077 g of thiourea were dissolved in 22 mL of ultrapure water under continuous stirring over 30 min. The transparent solution was transferred to a 50 mL Teflon-lined stainless steel autoclave. Treated CC was dipped in the autoclave, and the autoclave was maintained at 200 °C for 24 h in an oven. After autoclave cooled down to room temperature, the MoS_2-CC was obtained. The sample was washed with ultrapure water and ethanol for several times, and then dried at 60 °C for overnight.

Synthesis of Ni_3S_2/MoS_2-CC

Briefly, 16 mL of ethylenediamine was dissolved in 16 mL of ethanol and stirred for over 10 min. The transparent solution was transferred to a 50 mL Teflon-lined stainless steel autoclave. MoS_2-CC, 0.064g of sulfur powder, and 0.714 g of $NiCl_2{\cdot}6H_2O$ were placed in the autoclave. Then, the autoclave was sealed after ultrasonic for 10 min and maintained at 160 °C for 6 h in an oven. After autoclave cooled down to room temperature, the Ni_3S_2/MoS_2-CC was obtained. The sample was washed with ultrapure water and ethanol for several times, and then dried at 60 °C for overnight.

Synthesis of $NiFe(OH)_x$@Ni_3S_2/MoS_2-CC

The electrodeposition was carried out with three-electrode electrochemical cell containing Ni_3S_2/MoS_2-CC as the working electrode, platinum plate as the counter electrode and Ag/AgCl electrode in saturated KCl solution as the reference electrode. Electrolyte consisted of 80 mM $NiCl_2{\cdot}6H_2O$, 0.2 M $Na_3C_6H_5O_7{\cdot}2H_2O$, 0.45 M $(NH_4)_2SO_4$, and 0.55 M $NaPO_2H_2{\cdot}H_2O$. Subsequently, ultra-thin Ni film was fabricated through controlled current electrolysis under 5 mA cm^{-2} at room temperature using CHI660E potentiostat. The optimized Ni film deposition time has been determined to be 10 min. After deposition, the precursor with thin Ni film was carefully rinsed by water and acetone. Moreover, 0.101 g of $FeCl_3{\cdot}6H_2O$ and 0.212 g of $NaNO_3$ were dissolved in 50 mL of ultrapure water. The solution was heated at 100 °C for over 5 min. Then, the precursor was immersed in the hot solution and kept at 100 °C for 10 s. The final sample denoted as $NiFe(OH)_x$@Ni_3S_2/MoS_2-CC was washed with water and ethanol for several times and dried in vacuum overnight.

Synthesis of 20 wt % Pt/C-CC and RuO_2-CC

To fabricate Pt/C-CC, commercial 20 wt % Pt/C powder was firstly dispersed in 920 μL of solution with a ratio of v(H_2O)/v(ethanol) = 1/2, then 80 μL of Nafion was added. The mixture was sonicated over 20 min to obtain a homogeneous slurry. The slurry was coated onto a piece of treated CC with well-distribution and evaporated naturally under ambient conditions. RuO_2-CC was prepared by using commercial RuO_2 powder in the same procedure.

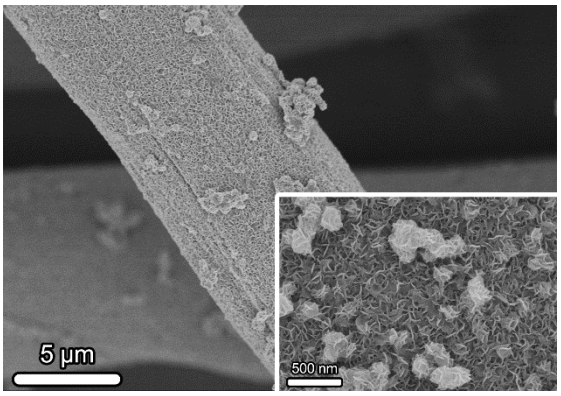

Fig. S1. SEM image of MoS_2-CC. The inset image shows the exterior nanosheets grown on carbon cloth.

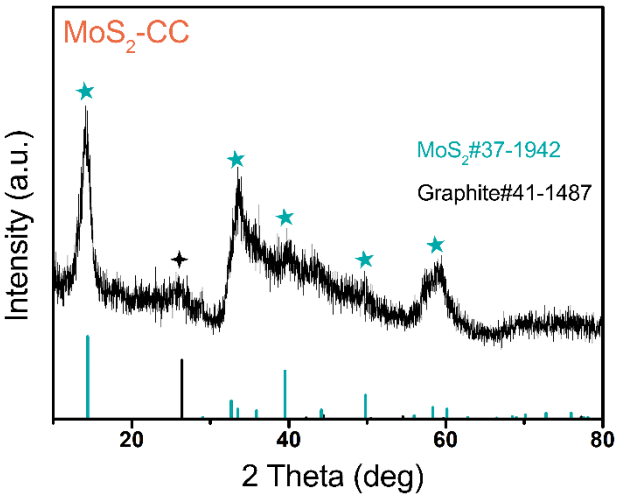

Fig. S2. XRD pattern of MoS_2-CC. Characteristic diffraction peaks of MoS_2 (JCPDS #37-1492) and graphite (JCPDS #41-1487) are clearly observed.

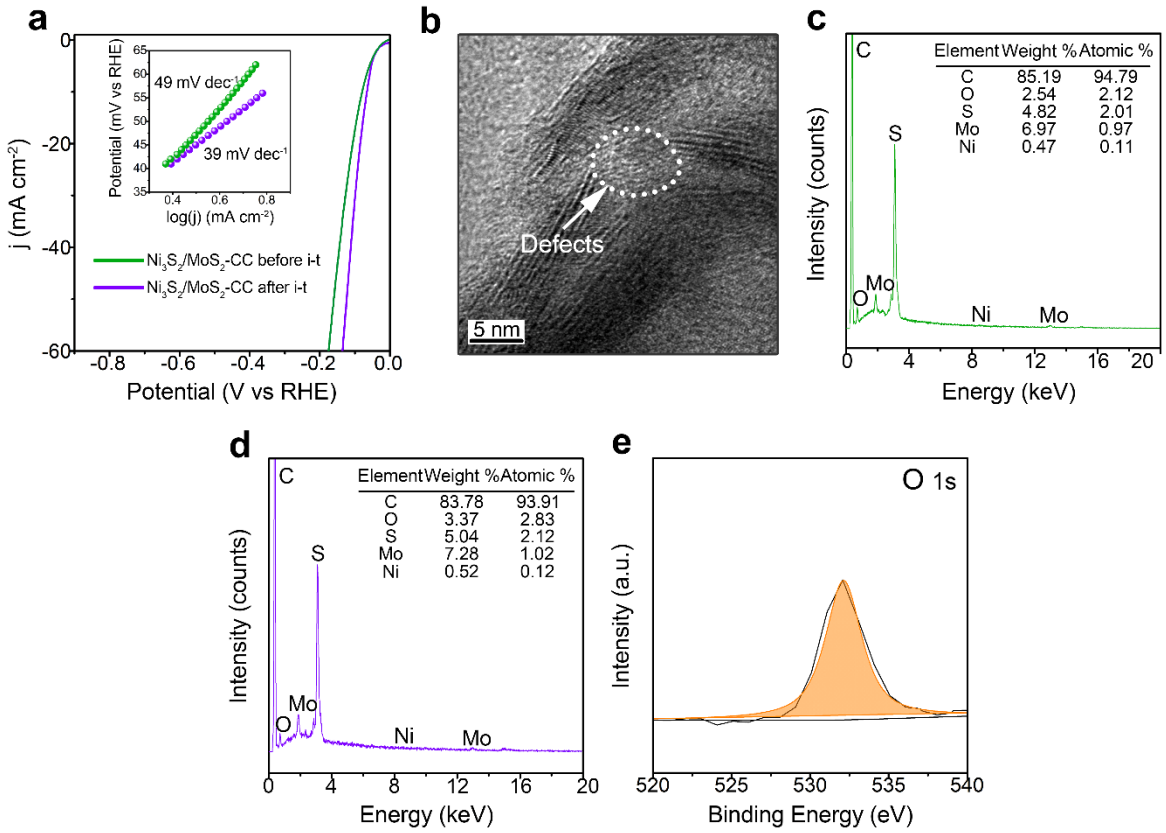

Fig. S3. (a) LSV curves of Ni_3S_2/MoS_2-CC before and after stability test. The inset displays the corresponding Tafel plots of Ni_3S_2/MoS_2-CC before and after stability test. (b) HRTEM image of Ni_3S_2/MoS_2-CC. (c) and (d) display the EDX spectra of the Ni_3S_2/MoS_2-CC before and after stability test, respectively. (e) High-resolution XPS spectrum of O 1s in the Ni_3S_2/MoS_2-CC.

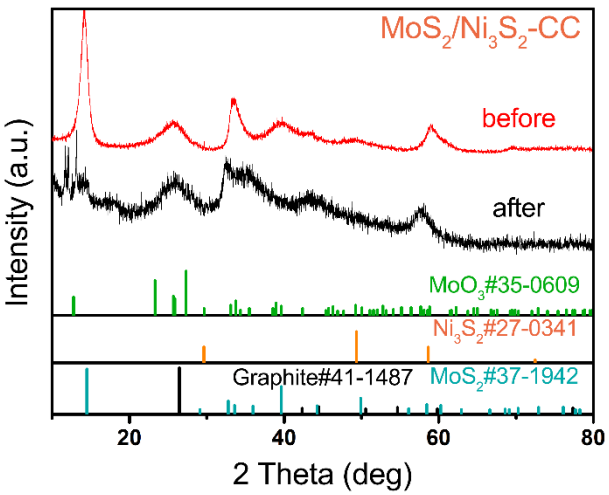

Fig. S4. XRD patterns of Ni_3S_2/MoS_2-CC catalyst before and after long-term HER electrolysis.

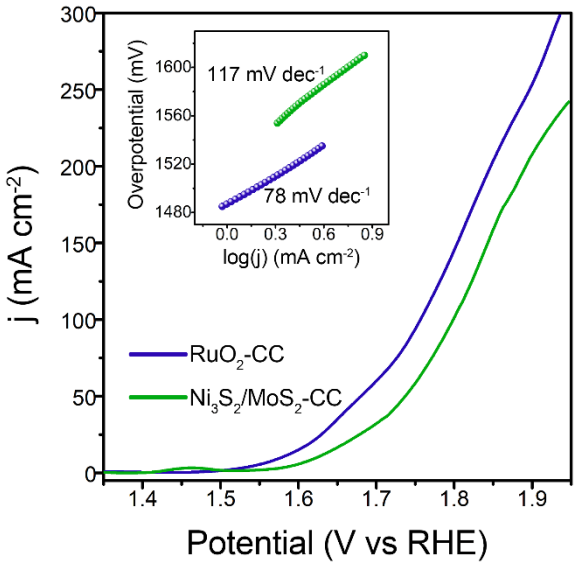

Fig. S5. LSV curves of the Ni_3S_2/MoS_2-CC catalyst and RuO_2-CC. The inset displays the Tafel plots (mV dec^{-1}) of Ni_3S_2/MoS_2-CC and RuO_2-CC.

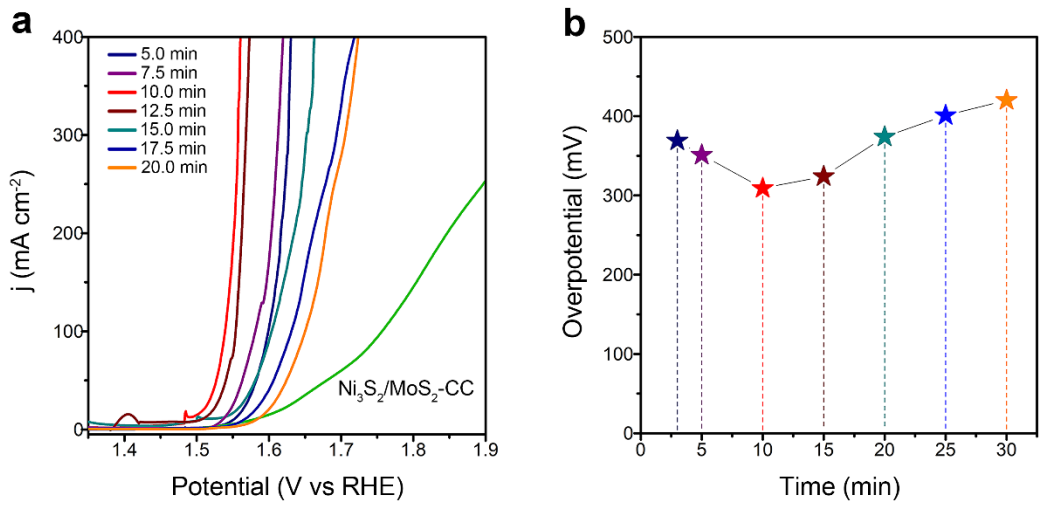

Fig. S6. (a) Diverse LSV curves of $NiFe(OH)_x@Ni_3S_2/MoS_2$-CC samples with different amounts of Ni at different deposition times in 1.0 M KOH. The amount of Fe involved in the reaction is fixed to be immersed in the pre-heated $FeCl_3/NaNO_3$ solution for 10 seconds. (b) Overpotentials of samples owned with different amounts of Ni.

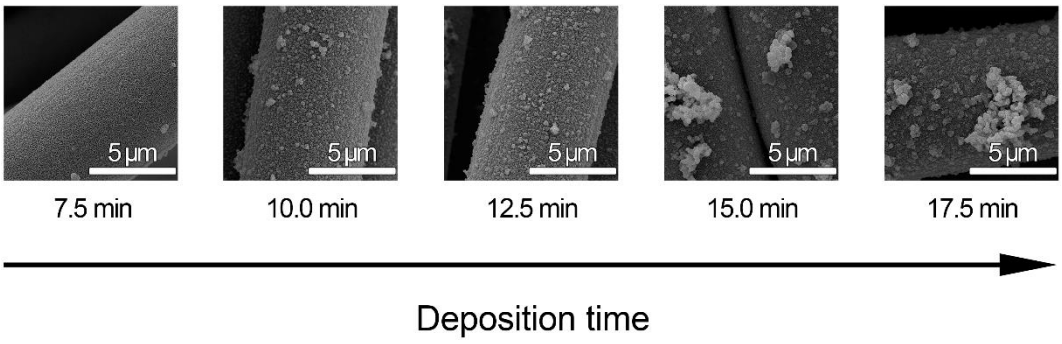

Fig. S7. SEM graphics of Ni@Ni_3S_2/MoS_2-CC samples with different deposition time of surface nickel.

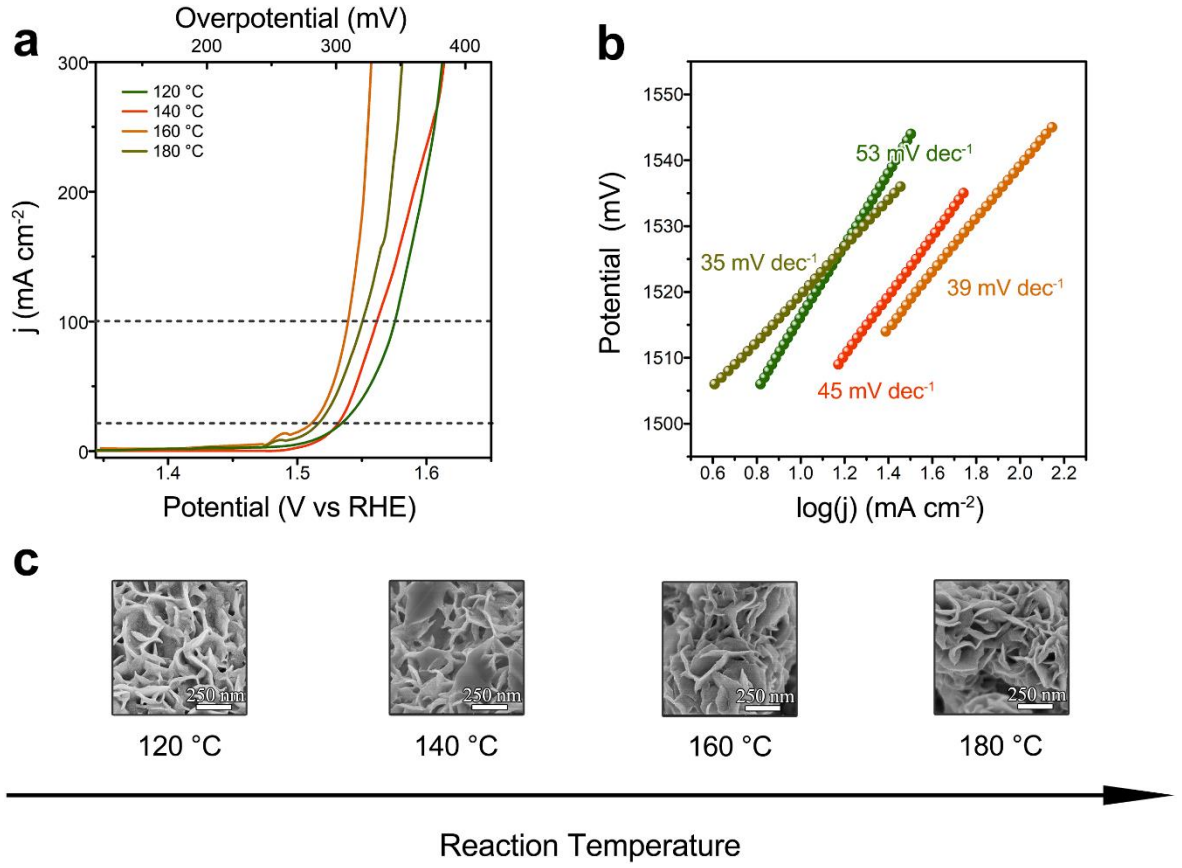

Fig. S8. (a, b) The LSV curves and corresponding Tafel plots of $NiFe(OH)_x@Ni_3S_2/MoS_2$-CC samples prepared at different temperatures (for the procedure of 2nd hydrothermal treatment) for OER. (c) The corresponding SEM graphics of Ni_3S_2/MoS_2-CC samples prepared at different temperatures (for the procedure of 2nd hydrothermal treatment).

The morphology of the nanosheets on the samples' surface is not changed significantly. The thin and dense NSs were grown in the vertical direction of CC substrate with a porous structure. From 120 °C to 160 °C, with increasing synthetic temperature, the overpotential reduced (100 mA cm^{-2}), the Tafel slope values decreased, and the overall intrinsic catalytic activity was improved. Sample prepared at 180 °C owns the lowest Tafel slope, but the overpotential is somewhat degraded when driving the high current density. Therefore, exorbitant reaction temperature is unnecessary to the promotion of the performance.

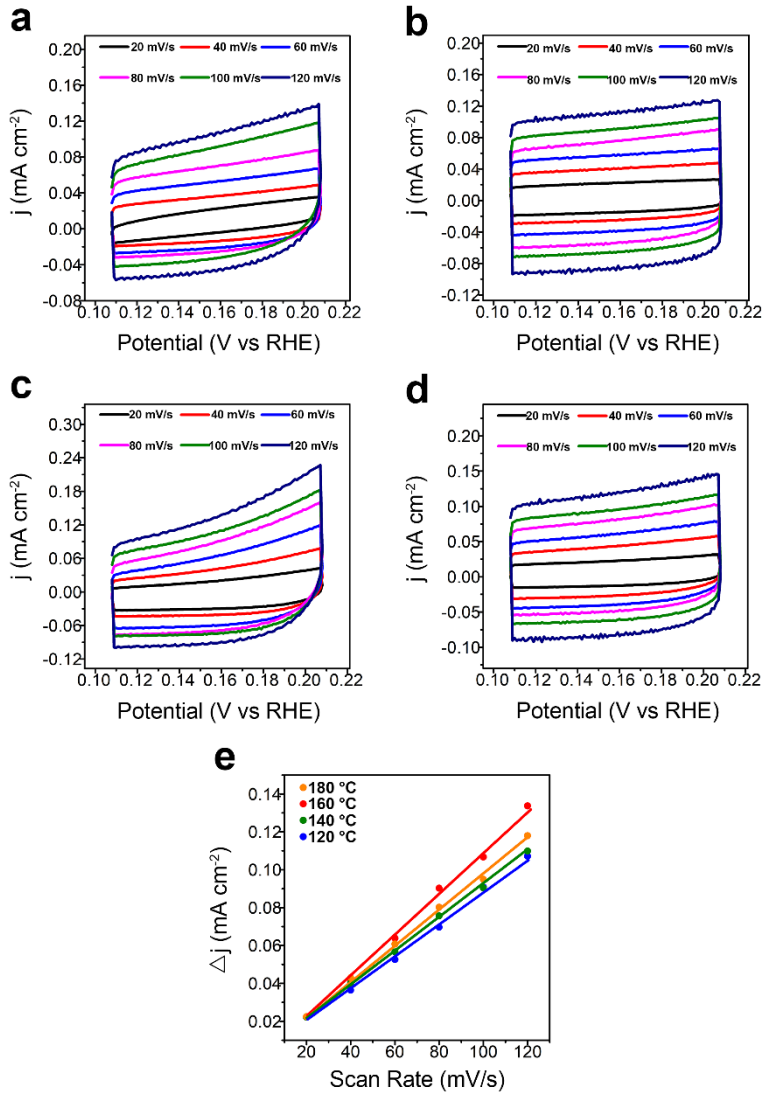

Fig. S9. Cyclic voltammetry curves of $NiFe(OH)_x@Ni_3S_2/MoS_2$-CC samples prepared at different reaction temperatures (for the procedure of 2nd hydrothermal treatment) of (a) 120 °C, (b) 140 °C, (c) 160 °C, and (d) 180 °C in 1 M KOH at various scanning rates (from 20 to 120 mV s^{-1}), within a potential range from 0.108 to 0.208 V vs. RHE. (e) Comparison of the double-layer capacitance (C_{dl}).

The CV measurements were executed to detect the electrochemical double layer capacitance (C_{dl}) of several samples at non-faraday cover potentials as the means of estimating the corresponding effective electrode surface areas (denoted as ECSA). As a result, the sample obtained at 160 °C is the best choice.

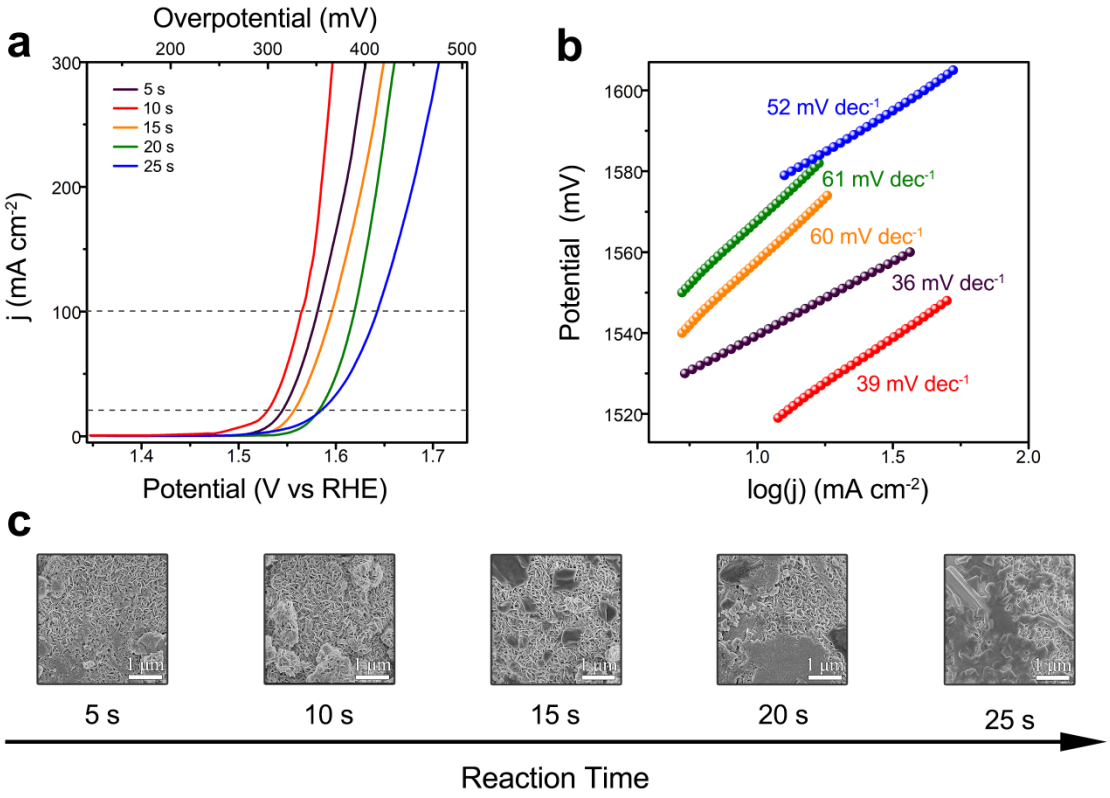

Fig. S10. (a, b) The LSV curves and corresponding Tafel plots of $NiFe(OH)_x@Ni_3S_2/MoS_2$-CC samples prepared with different reaction time (for the procedure of in-situ growth of metal hydroxides) for OER. (c) The corresponding SEM graphics of $NiFe(OH)_x@Ni_3S_2/MoS_2$-CC samples prepared with different reaction time (for the procedure of in-situ growth of metal hydroxides).

In-situ growth of metal hydroxides with different reaction time has a greater impact on performance than 2nd hydrothermal treatment. With the reaction time passing, the hydroxides covered more regions. Samples presented undulating values on Tafel slope. Long-term growth of hydroxides caused the decline of slope value and increase of overpotential.

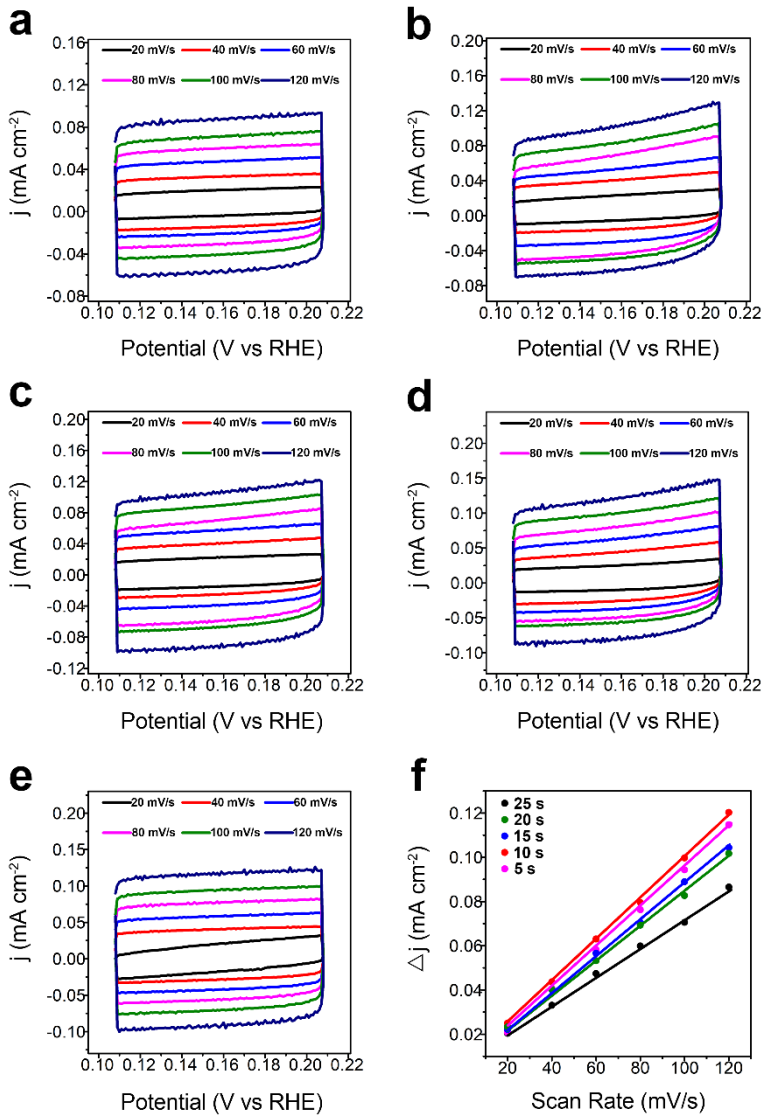

Fig. S11. Cyclic voltammograms of $NiFe(OH)_x@Ni_3S_2/MoS_2$-CC samples prepared at different reaction time (for the procedure of in-situ growth of metal hydroxides) of (a) 5 s, (b) 10 s, (c) 15 s, (d) 20 s, and (e) 25 s in 1 M KOH at various scanning rates (from 20 to 120 mV s^{-1}), within a potential range from 0.108 to 0.208 V vs. RHE. (f) Comparison of the double-layer capacitance (C_{dl}).

The C_{dl} values of the samples were measured and the slopes of the fitting lines were used for the determination of the C_{dl} that was proportional to the ECSA. Relatively long reaction time was needed to form uniform and fine nanostructure. Moreover, the slope of sample (25 s) is the lowest, revealing the ECSA decrease with overgrowth of metal hydroxides.

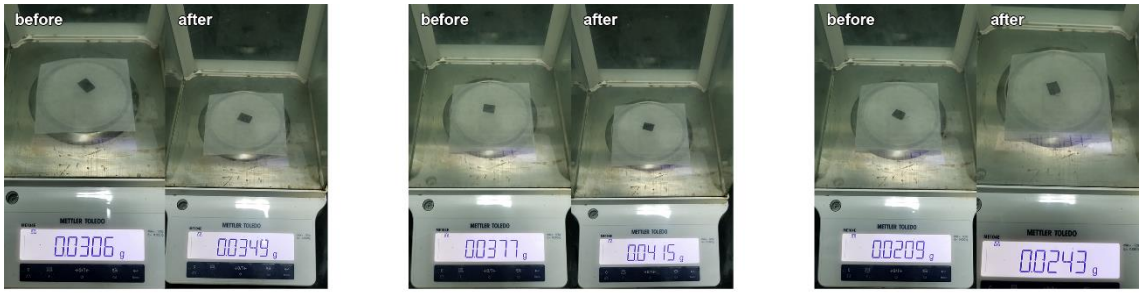

Fig. S12. The standard loading mass of $NiFe(OH)_x@Ni_3S_2/MoS_2$ catalysts on CC is obtained by averaging the weight differences (Δm) of the three samples. More precisely, the calculation of TOF values is based on the total loading mass of metal species on CC substrates.

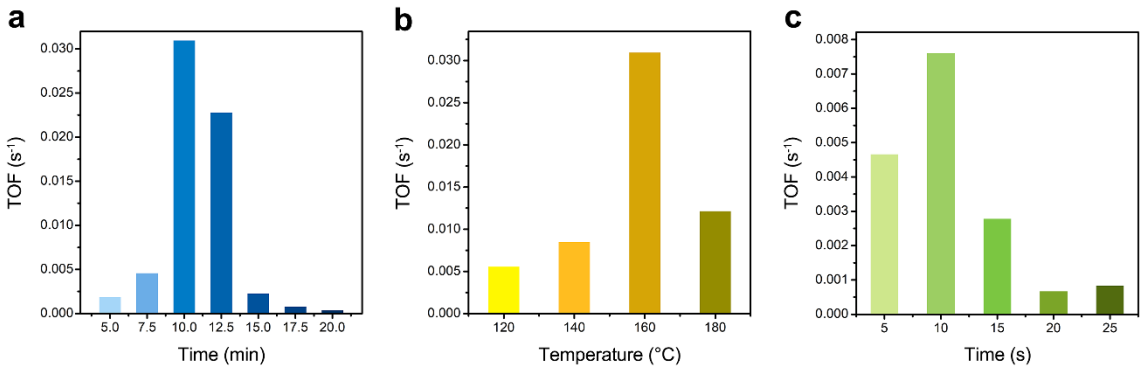

Fig. S13. TOF values of $NiFe(OH)_x@Ni_3S_2/MoS_2$-CC samples under different reaction conditions with (a) deposition time of Ni, (b) 2nd hydrothermal temperature, and (c) time of in-situ growth of metal hydroxides.

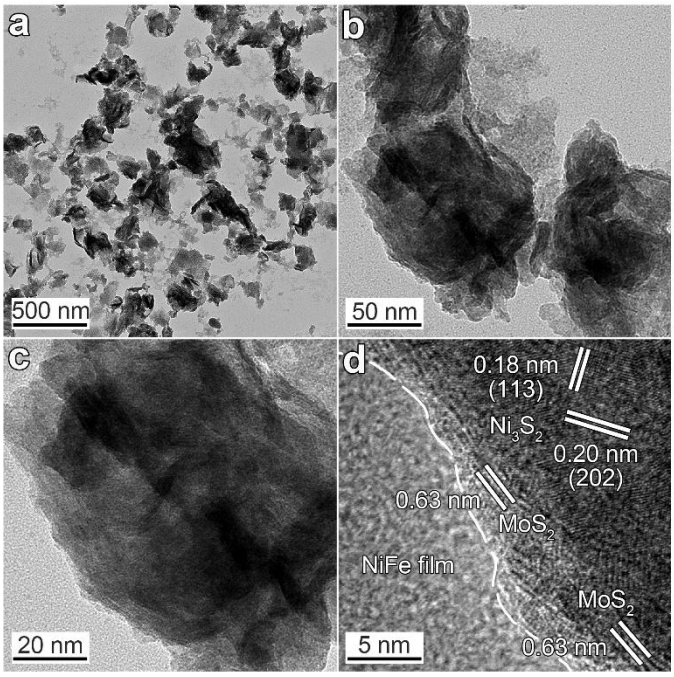

Fig. S14. TEM graphics of exfoliated $NiFe(OH)_x@Ni_3S_2/MoS_2$ in different resolutions.

Particularly, further amplified TEM image (d) shows a typical boundary area of TMSs and amorphous NiFe film. The marked interplanar spacings of 0.18, 0.20, and 0.63 nm can be clearly captured, which are identical with those of Ni_3S_2 (113), (202), and MoS_2, respectively. The area to the left of the white dotted line is the amorphous NiFe film.

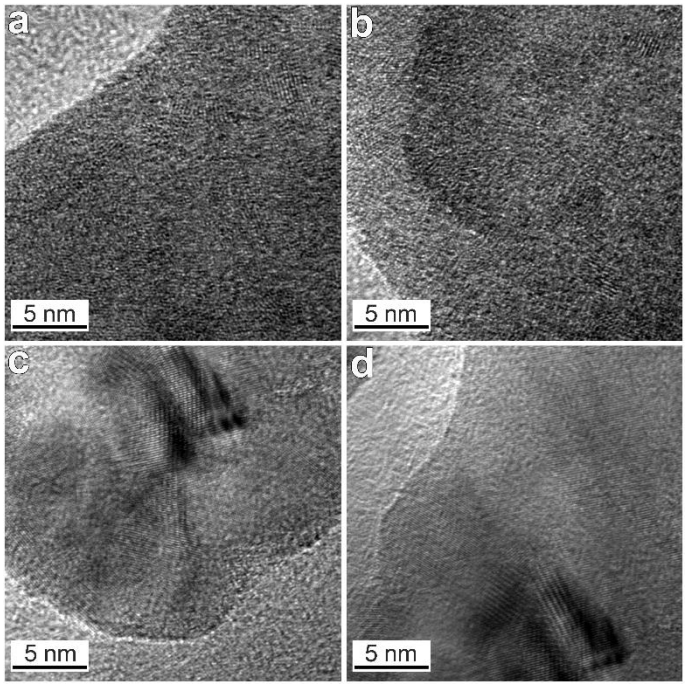

Fig. S15. TEM graphics of exfoliated $NiFe(OH)_x@Ni_3S_2/MoS_2$ with different regions (a-d) display the crystalline and amorphous phase in hierarchical nanostructure.

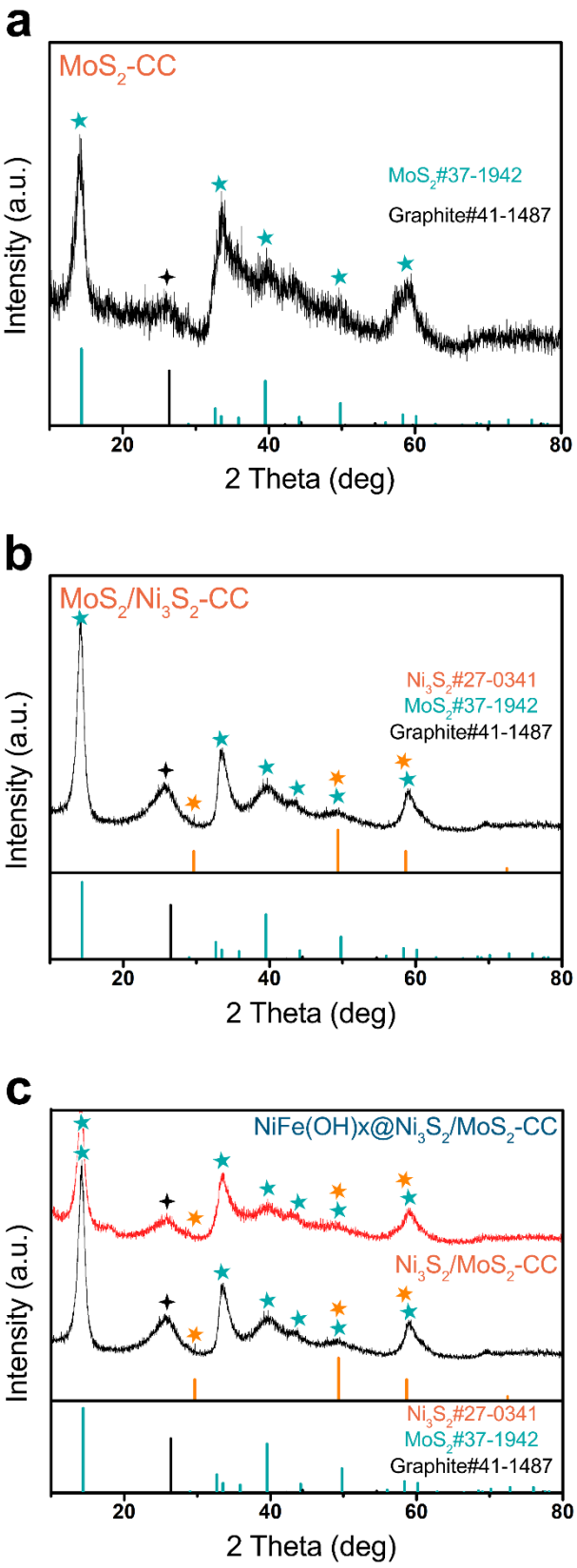

Fig. S16. XRD patterns of (a) MoS_2-CC, (b) Ni_3S_2/MoS_2-CC, and (c) $NiFe(OH)_x@Ni_3S_2/MoS_2$-CC.

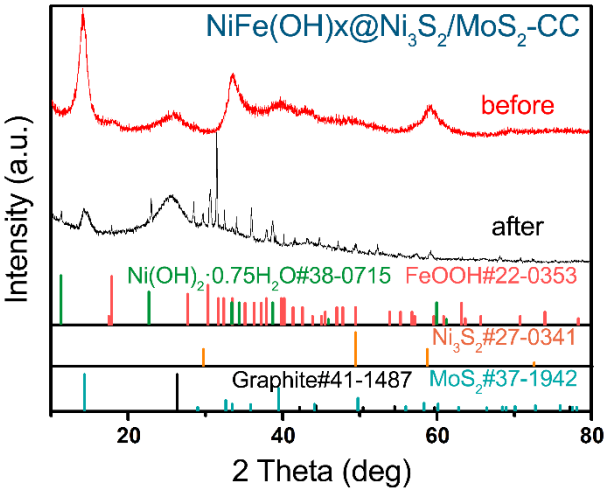

Fig. S17. XRD patterns of NiFe(OH)$_x$@Ni_3S_2/MoS_2-CC catalyst before and after long-term OER electrolysis.

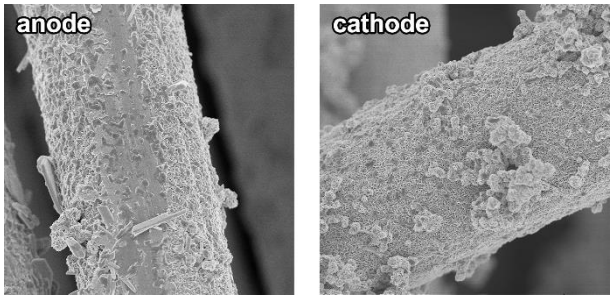

Fig. S18. SEM images of two electrodes after overall water electrolysis durability test.

Table S1. Mass-normalized HER performances of Ni_3S_2/MoS_2-CC and its comparatives.

Sample	Mass activity @η = 0.1 V (A g^{-1})	Mass activity @η = 0.2 V (A g^{-1})	Mass activity @η = 0.3 V (A g^{-1})
Ni_3S_2/MoS_2-CC	9.03	37.68	72.68
MoS_2-CC	0.12	1.67	16.04
Pt/C	17.53	56.86	106.71
bare CC	NA[a]	NA[a]	NA[a]

[a] NA stands for no catalytic material on the bare carbon cloth (CC), so there is no corresponding mass-normalized activity for bare CC sample.

Table S2. Comparison of the HER performance for the catalyst in this work with other reported electrocatalysts in 1 M alkaline electrolytes (KOH or NaOH).

Catalyst	Support	Current density *j* (mA cm^{-2})	Voltage at *the Corresponding j* (mV)	Electrolyte solution	Reference
Ni_3S_2/MoS_2-CC	Carbon cloth	10 100 400	65 174 342	1 M KOH	This work
$NiCo_2O_4$/NiFe LDH	Ni foam	10 100	192 440	1 M KOH	ACS Appl. Mater. Interfaces. **2017**, *9*, 1488.
CoSe/NiFe LDH	Exfoliated graphene foil	10	260	1 M KOH	Energy Environ. Sci. **2017**, *9*, 478.
NiFe/$NiCo_2O_4$	Ni foam	10 100	105 202	1 M NaOH	Adv. Funct. Mater. **2017**, *26*, 3515.
$Cu_{0.3}Co_{2.7}P$	Glassy carbon	10 100	220 445	1 M KOH	Adv. Energy Mater. **2017**, *7*, 1601555.
Ni/Mo_2C/porous C	Glassy carbon	10	179	1 M KOH	Chem. Sci. **2017**, *8*, 968.
Janus Co/CoP	N doped C membranes	10	135	1 M KOH	ACS Nano **2017**, *11*, 4358.
Janus Co/CoP	Ni foam	10	193	1 M KOH	Adv. Energy Mater. **2017**, *7*, 1602355.
$Ni_{12}P_5$	Ni foam	10 100	170 290	1 M KOH	ACS Catal., **2017**, *7*, 103.
Cu/CoS_x	Cu foam	10 100	134 267	1 M KOH	Adv. Mater. **2017**, *29*, 1606200.
Co_3O_4 microtube	Ni foam	10 100	170 285	1 M KOH	Angew. Chem., Int. Ed. **2017**, *56*, 1324.
VOOH hollow nanosphere	Ni plate	10 100	164 270	1 M NaOH	Angew. Chem., Int. Ed. **2017**, *56*, 573.
CoS/carbon nanotube	Carbon paper	10	190	1 M KOH	ACS Nano **2017**, *10*, 2342.
$NiCo_2S_4$ nanowire	Ni foam	10 100	210 350	1 M KOH	Adv. Funct. Mater. **2017**, *26*, 4661.
MoC/Mo_2C	Glassy carbon	10	120	1 M KOH	Chem. Sci. **2017**, *7*, 3399
CoO_x/N doped C	Glassy carbon	10	232	1 M KOH	J. Am. Chem. Soc. **2017**, *137*, 2688.
Exfoliated NiFe LDH/defective graphene	Glassy carbon	10	210	1 M KOH	Adv. Mater. **2017**, *29*, 1700017.

Table S3. Mass-normalized OER performances of $NiFe(OH)_x$@Ni_3S_2/MoS_2-CC and its comparatives.

Sample	Mass activity @η = 0.3 V (A g^{-1})	Mass activity @η = 0.4 V (A g^{-1})	Mass activity @η = 0.5 V (A g^{-1})
$NiFe(OH)_x$ @Ni_3S_2/MoS_2-CC	15.47	233.29	366.05
Ni_3S_2/MoS_2-CC	0.45	3.43	13.55
MoS_2-CC	0.52	1.02	3.19
RuO_2-CC	0.86	6.35	19.40
bare CC	NA[a]	NA[a]	NA[a]

[a] NA stands for no catalytic material on the bare carbon cloth (CC), so there is no corresponding mass-normalized activity for bare CC sample.

Table S4. Comparison of OER performance in 1 M KOH solution for $(Ni_{0.33}Co_{0.67})S_2$ NWs/CC with some representative non-precious metal catalysts reported.

Catalyst	Support	Current density *j* (mA cm^{-2})	Voltage at *the Corresponding j* (mV)	Electrolyte solution (1 M)	Reference
$NiFe(OH)_x$@ Ni_3S_2/MoS_2-CC	Carbon cloth	10 100 400	1484 1539 1560	KOH	This work
Ni-Fe-OH@Ni_3S_2/NF	Ni foam	10 100	1478 1613	KOH	Adv. Mater. **2017**, *29*, 1700404.
$Ni_3Fe(OH)_9$/NF	Ni foam	100	1683	KOH	Nat. Commun. **2015**, *6*, 6616.
NiFe LDH/NF	Ni foam	10	1553	NaOH	Science **2014**, *345*, 1593.
$Ni_xFe_{1-x}Se_2$-DO	Ni foam	10	1508	KOH	Nat. Commun. **2016**, *7*, 12324.
$NiFeO_x$/CFP	Carbon fiber	10	1593	KOH	Nat. Commun. **2015**, *6*, 7261.
FeNi-rGO LDH	rGO	10	1519	KOH	Angew. Chem., Int. Ed. **2014**, *126*, 7714.
NiFe-LDH/CNT	Carbon nanotube	5	1563	KOH	J. Am. Chem. Soc. **2013**, *135*, 8452.
$Ni_{50}Fe_{50}$-DAT	Ni plate	100	1613	NaOH	ACS Catal. **2016**, *6*, 1159.
$Ni_{2/3}Fe_{1/3}$-rGO	rGO	10	1523	KOH	ACS Nano **2015**, *9*, 1977.
Exfoliated NiFe LDH/defective graphene	Glassy carbon	10 100	1533 1638	KOH	Adv. Mater. **2017**, *29*, 1700017.
NiFe LDH	Ni plate	10 100	1553 1763	NaOH	J. Mater. Chem. A **2016**, *4*, 167.
Fe doped CoP	Ti foil	10 100	1543 1623	KOH	Adv. Mater. **2017**, *29*, 1602441.
Fe_xN	Graphene/Ni foam	10 100	1555 1603	KOH	ACS Catal. **2017**, *7*, 2025.
Co-N-P doped carbon	Exfoliated graphene foil	10 30	1600 1670	KOH	Adv. Mater. **2017**, *29*, 1604480.
FeOOH/Co/FeOOH	Ni foam	100	1623	KOH	Angew. Chem., Int. Ed. **2017**, *55*, 3694.
$CoNi(OH)_x$	Cu foil	10 100	1593 1653	KOH	Adv. Energy Mater. **2017**, *6*, 1501661.

Table S5. Comparison of bifunctional electrocatalysts for overall water splitting in 1 M KOH solution.

Catalyst	Support	Current density *j* (mA cm^{-2})	Voltage at *the Corresponding j* (mV)	Electrolyte solution (1 M)	Reference
CMN//CMNF	carbon cloth	10	1.55	KOH	This work
Co_xMo_y@NC	glassy carbon	10	1.74	KOH	J. Mater. Chem. A **2017**, *5*, 16929
$Ni_{1.5}Fe_{0.5}P$/CF	carbon fiber	10 20	1.589 1.635	KOH	Nano Energy **2017**, *34*, 472.
Ni_2P	Ni foam	10	1.63	KOH	Energy Environ. Sci. **2015**, *8*, 2347.
Co-doped $NiSe_2$	Ti foam	10	1.62	KOH	Nanoscale **2016**, *8*, 3911.
(Ni, Co)Se_2-GA	Ni foam	10	1.60	KOH	ACS Catal. **2017**, *7*, 6394.
Ni_2Se/NF	Ni foam	10	1.63	KOH	Angew. Chem., Int. Ed. **2015**, *54*, 9351.
$Co_{0.85}Se$/NiFe-LDHs	graphene foil	20	1.71	KOH	Energy Environ. Sci. **2016**, *9*, 478.
NiFe/$NiCo_2O_4$	Ni foam	10	1.67	KOH	Adv. Funct. Mater. **2016**, *26*, 3515.
N-Ni_3S_2	Ni foam	10	1.48	KOH	Adv. Mater. **2017**, *29*, 1701584.

Movie S1. This movie displays NMC//NFNMC AWSD operated at a large current density of 50 mA cm^{-2} to drive overall water splitting. Generated hydrogen and oxygen gases are efficiently and rapidly released from the electrodes.

References

1. Z. Q. Wang, S. Zeng, W. H. Liu, X. W. Wang, Q. W. Li, Z. G. Zhao and F. X. Geng, *ACS Appl. Mater. Inter.*, 2017, **9**, 1488-1495.
2. Y. Hou, M. R. Lohe, J. Zhang, S. H. Liu, X. D. Zhuang and X. L. Feng, *Energy Environ. Sci.*, 2016, **9**, 478-483.
3. C. L. Xiao, Y. B. Li, X. Y. Lu and C. Zhao, *Adv. Funct. Mater*, 2016, **26**, 3515-3523.
4. J. H. Song, C. Z. Zhu, B. Z. Xu, S. F. Fu, M. H. Engelhard, R. F. Ye, D. Du, S. P. Beckman and Y. H. Lin, *Adv. Energy Mater.*, 2017, **7**, 1601555.
5. Z. Y. Yu, Y. Duan, M. R. Gao, C. C. Lang, Y. R. Zheng and S. H. Yu, *Chem. Sci.*, 2017, **8**, 968-973.
6. H. Wang, S. X. Min, Q. Wang, D. B. Li, G. Casillas, C. Ma, Y. Y. Li, Z. X. Liu, L. J. Li, J. Y. Yuan, M. Antonietti and T. Wu, *ACS Nano*, 2017, **11**, 4358-4364.
7. Z. H. Xue, H. Su, Q. Y. Yu, B. Zhang, H. H. Wang, X. H. Li and J. S. Chen, *Adv. Energy Mater.*, 2017, **7**, 1602355.
8. P. W. Menezes, A. Indra, C. Das, C. Walter, C. Gobel, V. Gutkin, D. Schmeisser and M. Driess, *ACS Catal.*, 2017, **7**, 103-109.
9. Y. P. Liu, Q. J. Li, R. Si, G. D. Li, W. Li, D. P. Liu, D. J. Wang, L. Sun, Y. Zhang and X. X. Zou, *Adv Mater*, 2017, **29**, 1606200.
10. Y. P. Zhu, T. Y. Ma, M. Jaroniec and S. Z. Qiao, *Angew. Chem. Int. Edit.*, 2017, **56**, 1324-1328.
11. H. H. Shi, H. F. Liang, F. W. Ming and Z. C. Wang, *Angew. Chem. Int. Edit.*, 2017, **56**, 573-577.
12. J. Wang, H. X. Zhong, Z. L. Wang, F. L. Meng and X. B. Zhang, *ACS Nano*, 2016, **10**, 2342-2348.
13. A. Sivanantham, P. Ganesan and S. Shanmugam, *Adv. Funct. Mater.*, 2016, **26**, 4661-4672.
14. H. L. Lin, Z. P. Shi, S. N. He, X. Yu, S. N. Wang, Q. S. Gao and Y. Tang, *Chem. Sci.*, 2016, **7**, 3399-3405.
15. H. Y. Jin, J. Wang, D. F. Su, Z. Z. Wei, Z. F. Pang and Y. Wang, *J. Am. Chem. Soc.*, 2015, **137**, 2688-2694.
16. Y. Jia, L. Z. Zhang, G. P. Gao, H. Chen, B. Wang, J. Z. Zhou, M. T. Soo, M. Hong, X. C. Yan, G. R. Qian, J. Zou, A. J. Du and X. D. Yao, *Adv. Mater.*, 2017, **29**, 1700017.

17. X. Zou, Y. P. Liu, G. D. Li, Y. Y. Wu, D. P. Liu, W. Li, H. W. Li, D. J. Wang, Y. Zhang and X. X. Zou, *Adv. Mater.*, 2017, **29**, 1700404.
18. X. Y. Lu and C. A. Zhao, *Nat. Commun.*, 2015, **6**, 6616.
19. J. S. Luo, J. H. Im, M. T. Mayer, M. Schreier, M. K. Nazeeruddin, N. G. Park, S. D. Tilley, H. J. Fan and M. Gratzel, *Science*, 2014, **345**, 1593-1596.
20. X. Xu, F. Song and X. L. Hu, *Nat. Commun.*, 2016, **7**, 12324.
21. H. T. Wang, H. W. Lee, Y. Deng, Z. Y. Lu, P. C. Hsu, Y. Y. Liu, D. C. Lin and Y. Cui, *Nat. Commun.*, 2015, **6**, 7261.
22. M. Gong, Y. G. Li, H. L. Wang, Y. Y. Liang, J. Z. Wu, J. G. Zhou, J. Wang, T. Regier, F. Wei and H. J. Dai, *J. Am. Chem. Soc.*, 2013, **135**, 8452-8455.
23. T. T. H. Hoang and A. A. Gewirth, *ACS Catal.*, 2016, **6**, 1159-1164.
24. W. Ma, R. Z. Ma, C. X. Wang, J. B. Liang, X. H. Liu, K. C. Zhou and T. Sasaki, *ACS Nano* **2015**, 9, 1977-1984.
25. X. G. Liu, X. Wang, X. T. Yuan, W. J. Dong and F. Q. Huang, *J. Mater. Chem. A* **2016**, 4, 167-172.
26. C. Tang, R. Zhang, W. B. Lu, L. B. He, X. Jiang, A. M. Asiri and X. P. Sun, *Adv. Mater.* **2017**, 29, 1602441.
27. Y. Hou, M. Qiu, T. Zhang, J. Ma, S. H. Liu, X. D. Zhuang, C. Yuan and X. L. Feng, *Adv. Mater.* **2017**, 29, 1604480.
28. J. X. Feng, H. Xu, Y. T. Dong, S. H. Ye, Y. X. Tong and G. R. Li, *Angew. Chem., Int. Edit.* **2016**, 55, 3694-3698.
29. S. W. Li, Y. C. Wang, S. J. Peng, L. J. Zhang, A. M. Al-Enizi, H. Zhang, X. H. Sun and G. F. Zheng, *Adv. Energy Mater.* **2016**, 6, 1501661.
30. J. Jiang, Q. X. Liu, C. M. Zeng and L. H. Ai, *J. Mater. Chem. A* **2017**, 5, 16929-16935.
31. H. W. Huang, C. Yu, C. T. Zhao, X. T. Han, J. Yang, Z. B. Liu, S. F. Li, M. D. Zhang and J. S. Qiu, *Nano Energy*, 2017, **34**, 472-480.
32. L. A. Stern, L. G. Feng, F. Song and X. L. Hu, *Energy Environ. Sci.*, 2015, **8**, 2347-2351.
33. T. T. Liu, A. M. Asiri and X. P. Sun, *Nanoscale*, 2016, **8**, 3911-3915.
34. X. Xu, H. F. Liang, F. W. Ming, Z. B. Qi, Y. Q. Xie and Z. C. Wang, *ACS Catal.*, 2017, **7**, 6394-6399.
35. C. Tang, N. Y. Cheng, Z. H. Pu, W. Xing and X. P. Sun, *Angew. Chem., Int. Edit.* **2015**, 54, 9351-9355.

36. Y. Hou, M. R. Lohe, J. Zhang, S. H. Liu, X. D. Zhuang and X. L. Feng, *Energy Environ Sci*, 2016, **9**, 478-483.
37. C. L. Xiao, Y. B. Li, X. Y. Lu and C. Zhao, *Adv. Funct. Mater.* **2016**, 26, 3515-3523.
38. P. Z. Chen, T. P. Zhou, M. X. Zhang, Y. Tong, C. G. Zhong, N. Zhang, L. D. Zhang, C. Z. Wu and Y. Xie, *Adv. Mater.*, 2017, **29**, 1701584.